Journal Name

COMMUNICATION

Highly Active Hydrogen Evolution Catalysis from Metallic WS₂ Nanosheets

Mark A. Lukowski,[a] Andrew S. Daniel,[a] Caroline R. English,[a] Fei Meng,[a] Audrey Forticaux,[a] Robert J. Hamers,[a] and Song Jin[a*]

We report metallic WS₂ nanosheets that display excellent catalytic activity for the HER that is the best reported for MX₂ materials. They are chemically exfoliated from WS₂ nanostructures synthesized by chemical vapour deposition, including by using a simple and fast microwave-assisted intercalation method. Structural and electrochemical studies confirm that the simultaneous conversion and exfoliation of semiconducting 2H-WS₂ into nanosheets of its metallic 1T polymorph result in facile electrode kinetics, excellent electrical transport, and proliferation of catalytic active sites.

The need to replace rare and expensive noble metal catalysts with earth-abundant materials continues to be a strong driving force behind current research in sustainable energy technologies.[1] For producing hydrogen fuel in the hydrogen evolution reaction (HER), layered group 6 metal chalcogenides (MX₂; M = Mo, W; X= S, Se) are an exciting family of catalysts.[2] Their structures consist of two-dimensional (2D) covalently-bonded layers that are stacked to form hexagonal structures held together by weak van der Waals interactions. Experimental[3] and computational[4] studies show catalytically active sites are located along the edges of the 2D MX₂ layers while the basal surfaces are catalytically inert. Although molybdenum disulfide (MoS₂) is more well known as an HER catalyst, the analogous tungsten disulfide (WS₂) also exhibits promising activity.[2b, 5] Not surprisingly, WS₂ suffers from many of the same issues that have limited the HER performance of MoS₂, including low density and reactivity of active sites and poor electrical contact of the catalyst to its support.[2] These general challenges in MX₂ electrocatalysis have been addressed by recent advances that show the HER catalytic activity can be significantly enhanced when the semiconducting MoS₂ or WS₂ are chemically exfoliated into metallic nanosheets.[6] However, the performance of

Broader context

The scalable and sustainable production of hydrogen fuel through water splitting demands efficient and robust earth-abundant electrocatalysts for the hydrogen evolution reaction (HER). Layered chalcogenide materials, such as MoS₂ and WS₂, are promising earth-abundant alternative electrocatalysts to noble metals for hydrogen evolution reaction (HER), but their catalytic performance still needs to be improved. Here we develop metallic WS₂ nanosheets that show extraordinary catalytic activity for the HER via facile chemical exfoliation from WS₂ nanostructures synthesized by chemical vapour deposition, including by using a simple and fast microwave-assisted intercalation reaction method. The structural and chemical changes that take place during the exfoliation of the WS₂ nanosheets explain their excellent attributes and result in high electrocatalytic current density at low catalytic overpotential, which is the best HER performance reported for MX₂ catalysts.

WS₂ nanosheets still lags behinds that of the MoS₂ analog. Here we develop metallic WS₂ nanosheets that display extraordinary catalytic activity for the HER via facile preparation methods, including by using a simple and short microwave-assisted intercalation reaction. These solution processable exfoliated catalysts that can be dropcasted onto any inert conducting substrates are capable of achieving an electrocatalytic current density of 10 mA/cm² at the low potential of –142 mV vs. RHE, which is the best HER performance reported for MX₂ catalysts.

Our strategy begins with the chemical vapour deposition (CVD) synthesis of flower-like WS₂ nanostructures with a high density of exposed edges. Similar to our previously reported CVD method for producing MoS₂ nanostructures,[6a] the mild synthesis conditions around 550 °C (see SI for experimental details) make the deposition

of WS_2 possible on many different substrates, including graphite, tungsten foil, and fluorine-doped tin oxide/glass. Moreover, these WS_2 nanostructures with a thickness of about 10 layers are dominated by well-defined crystalline edges, thus increasing the density of active sites (Fig. 1b). Lattice resolved high-resolution transmission electron microscopy (HRTEM) show highly crystalline multilayered platelets (Fig. 1c) that, importantly, do not form closed fullerene-like structures (Fig. 1d). The corresponding selected-area electron diffraction (SAED) pattern is unequivocally indexed to 2H-WS_2 (Fig. 1e). The phase identity of the as-synthesized WS_2 nanostructures is further confirmed using Raman spectroscopy and powder X-ray diffraction (PXRD) (Fig. S1).
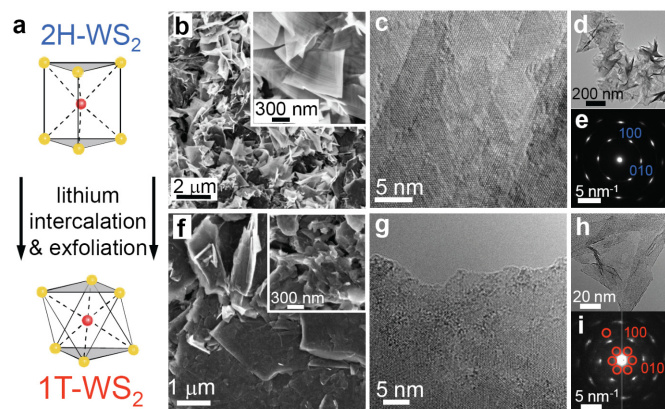

Fig. 1 (a) Simple intercalation chemistry is used to drive the phase transformation from the 2H- to the 1T-WS_2 polymorph. Top-down SEM images of the (b) as-grown WS_2 nanostructures on W foil and (f) chemically exfoliated nanosheets cast on graphite. Insets illustrate the high density of exposed edges. HRTEM of the (c) as-grown nanostructures and (g) exfoliated nanosheets. Lower resolution images (d, h) confirm they are open structures rather than inorganic fullerenes and electron diffraction patterns confirm the phase identity for the (e) 2H-WS_2 nanostructures and (i) 1T-WS_2 nanosheets.

We then use simple lithium intercalation chemistry to control the structural polymorphs in WS_2 materials.[7] Lithium intercalation of MX_2 materials can be accomplished through either chemical (using *n*-butyllithium)[6a-c, 8] or electrochemical methods.[6d, 9] Reduction by the butyllithium reagent during the intercalation reaction destabilizes the semiconducting and thermodynamically favored trigonal prismatic 2H structure, causing a transition to the octahedral 1T polymorph (Fig. 1a). The intercalated layered material is chemically exfoliated upon reaction with excess water, which generates H_2 and produces individual 1T-WS_2 nanosheets. It is important to note that other exfoliation methods, such as mechanical cleavage or liquid-phase sonication, are limited to isolating nanosheets of the semiconducting 2H phase in low yield.[7] Here, we initially converted the as-grown 2H-WS_2 nanostructures to the metallic 1T-WS_2 polymorph by heating the samples immersed in *n*-butyllithium solution at 80 °C for 48 hours in sealed vials. The slightly higher temperature used here facilitates the intercalation process, which is known to be more difficult for WS_2 than MoS_2.[10] We further developed a new microwave-assisted reaction method to dramatically expedite the intercalation process (see SI for experimental details).[11] Remarkably, we found the chemically

exfoliated 1T-WS_2 nanosheets produced after only 20 min of microwave-assisted intercalation are nearly equivalent to those produced after 48 hours of heating in an oven. The shorter reaction time is also beneficial because WS_2 nanosheets appear to be more prone to oxidation than the MoS_2 nanosheets.[10]

However, we observed surprisingly different behaviour in the exfoliation of WS_2 nanosheets from that of MoS_2.[6a] Specifically, the violent generation of H_2 causes the exfoliated nanosheets to delaminate from graphite (and other) substrates, and this is especially severe for W foil substrates. Thus, such delamination prevented us from directly exfoliating WS_2 nanostructures grown on graphite and effectively testing their catalytic activity. In fact, the delamination of the WS_2 materials during exfoliation process was so severe that the initially attained HER catalytic performance was even worse than the as grown 2H-WS_2 on graphite substrate (Figure S5 in ESI). To overcome this obstacle, we took the opposite approach and harvested the WS_2 nanostructures grown on tungsten foil that were released from the substrate during the exfoliation treatment in a good yield. These harvested nanosheets can then be simply drop-casted onto any substrate, increasing the flexibility of electrode preparation. This approach not only allows us to achieve excellent catalytic performance as discussed below, but also minimizes waste, as the growth substrate can be cleaned and re-used in subsequent reactions. This newly developed "harvest and dropcast" approach can also be used to improve the preparation of metallic MoS_2 nanosheets with good HER performance.[6a]

We focus the structural characterization discussions on such drop-casted WS_2 nanosheets. SEM shows a uniform drop-casted film composed of many smaller sheets and particles covering a graphite disk (Fig. 1f). HRTEM (Fig. 1g) shows the more disordered structure of exfoliated nanosheets and confirms they are still open structures (Fig. 1h). The superlattice structure observed in the SAED pattern (red circles in Fig. 1i) is consistent with past reports of chemically exfoliated WS_2[5d, 12] and suggests the product may be a mixture of 1T- and 2H-WS_2.

We further characterized the 1T-WS_2 nanosheets to highlight their differences from the as grown 2H-WS_2 nanostructures using X-ray photoelectron spectroscopy (XPS), ultraviolet photoelectron spectroscopy (UPS), current-sensing atomic force microscopy (CSAFM), Raman spectroscopy, and PXRD. Fig. 2a and 2b show high-resolution XP spectra of the W4*f* (Fig. 2a) and S2*p* (Fig. 2b) regions, respectively. As a visual aid, black dotted lines have been added to bisect the W4$f_{7/2}$, W4$f_{5/2}$, and W5$p_{3/2}$ peaks in the 2H-WS_2 spectrum in Fig. 2a and the three peaks present in the 2H-WS_2 S2*p* spectrum in Fig. 2b. The 1T-WS_2 sample displays the presence of new chemical species clearly shifted toward lower binding energies after chemical exfoliation in both the W4*f* and S2*p* regions. These results are consistent with the known metallic nature of 1T-WS_2 and similar to past XPS studies on 1T-MX_2 materials.[6c, 8c, 13] The small shoulder at ~35 eV corresponding to a W4$f_{7/2}$ species (Fig. 4a) confirms that the exfoliated 1T-WS_2 nanosheets are more susceptible to oxidation.[10] In general, WS_2 samples appear to be more susceptible to oxidation than MoS_2 and there were minor variations in the degree of oxidation from sample to sample, depending on how well the reaction vessels were sealed during the exfoliation. The underlying Au substrate was used to manually align all XP spectra and the C1*s* data from the adventitious carbon for each sample were compared to rule out charging effects (see more details in SI and Fig.

S2). The more metallic character of the exfoliated nanosheets is also reflected in the UPS spectra (Fig. 2c, 2d). The 1T-WS$_2$ nanosheets exhibit a valence band maximum (VBM) at 0.3 eV, which is much closer to the Fermi level (defined here as 0 eV) than the 0.9 eV VBM observed for the 2H-WS$_2$ nanostructures. We also used CSAFM to confirm the semiconducting-to-metallic phase transition. Contact mode topography (Fig. 2g, 2h), friction, and deflection images (Fig. S3) show the presence of material cast onto an evaporated gold film on silicon substrate. Conductivity maps taken at +20 mV sample bias show the 2H-WS$_2$ nanostructures are much more resistive (Fig. 2e) than the more uniformly conducting 1T-WS$_2$ nanosheets (Fig. 2f). Individual current–voltage sweeps on specific nanostructures further contrast the clear differences in conductivity observed for the 1T- and 2H-WS$_2$ samples (Fig. 2i). Raman spectra of WS$_2$ show less distinctive peaks after phase transition (Fig. S1), but the characteristic peaks for the 2H phase are much less intense and significantly broadened, which is in agreement with previous reports[14] and similar to our own study of 1T-MoS$_2$. Given the more difficult intercalation reaction and the propensity of exfoliated WS$_2$ nanosheets to restack into their thermodynamically favoured 2H phase,[12b, 12c] it is likely that both the 1T and 2H polymorphs coexist in these exfoliated samples. PXRD supports this hypothesis, showing weakened reflections corresponding to the 2H polymorph (Fig. S1).
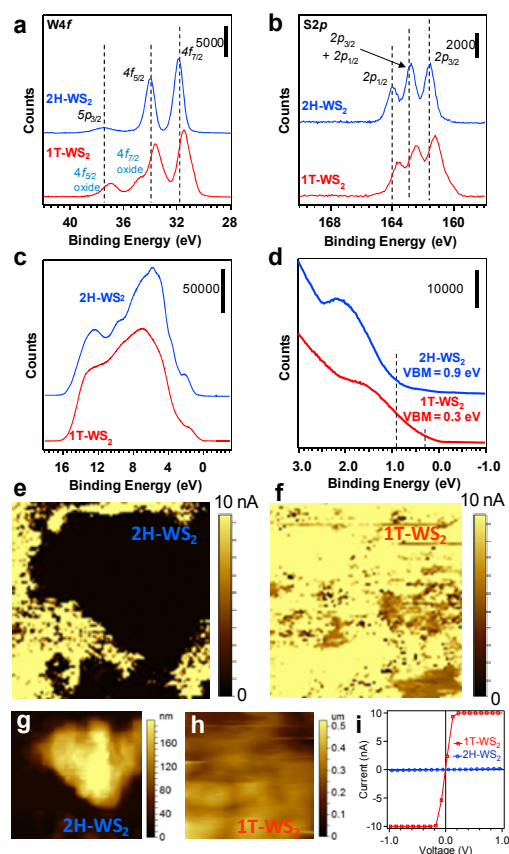

Fig. 2 Comparison of the as-grown 2H- and exfoliated 1T-WS$_2$ nanosheets. High resolution XP spectra of the (a) W4f and (b) S2p regions, showing a new chemical species exhibiting a clear shift to lower binding energies after chemical exfoliation. (c) Overall UP spectra and (d) zoom-in of the low binding energy edge of the UP spectra showing the valence band maxima with respect to the Fermi Level. (e-h) CSAFM micrographs and corresponding conductivity maps for the as-grown (e, g) and exfoliated (f,h) WS$_2$ nanosheets. All images are 2 μm by 2 μm and the conductivity maps were taken at a +20 mV bias. (i) Current–voltage curves on individual nanostructures, further contrasting the differences in conductivity.

We demonstrate that the metallic WS$_2$ nanosheets produced by our chemical exfoliation treatment exhibit extraordinary catalytic activity for the HER. We dropcasted the exfoliated 1T-WS$_2$ nanosheets (a total volume of 6 μL suspension) onto graphite disks and evaluated their catalytic activity in 0.5 M H$_2$SO$_4$ using a standard rotating disk electrode (RDE) apparatus in a three-electrode electrochemical measurement (see experimental details in the SI). The total mass of the deposited 1T-WS$_2$ nanosheets is quite small and using quartz crystal microbalance measurements we estimated that the amount of the WS$_2$ nanosheets loading to be 1.0±0.2 mg/cm^2 (see ESI for more details). Polarization curves (Fig. 3a) of the electrocatalytic current density (j) plotted against potential vs. the reversible hydrogen electrode (RHE) show the HER activity of 1T-WS$_2$ nanosheets obtained from both oven and microwave-assisted intercalation methods compared to the as-grown WS$_2$ nanostructures. As-grown WS$_2$ on graphite exhibits an onset of HER activity at approximately –200 mV vs. RHE and significant hydrogen evolution (j = 10 mA/cm^2) is not reached until –330 mV vs. RHE. Drop-casted 1T-WS$_2$ nanosheets that have been exfoliated after lithium intercalation at 80 °C for 48 h in an oven show dramatically improved HER activity, where the onset of catalytic activity has been shifted to significantly lower voltages of about –75 mV vs. RHE. After correcting for iR losses, these 1T-WS$_2$ nanosheets achieve an electrocatalytic current density of 10 mA/cm^2 at an unprecedented low overpotential of –142 mV vs. RHE (purple trace). This exceptional catalytic activity is further highlighted in Fig. 3a by comparing the 1T-WS$_2$ nanosheets against other recently reported high performing HER MX$_2$ catalysts of various morphologies and chemistry.[2, 6, 15] Interestingly, unlike MoS$_2$, WS$_2$ in its original semiconducting form is not well known as a good HER catalyst, but the best catalytic performance is achieved for the metallic WS$_2$ nanosheets here. The 1T-WS$_2$ nanosheets here are also significantly improved from both the previously reported 1T-WS$_2$ nanosheets exfoliated from commercial powers (green trace)[6c] and the 1T-MoS$_2$ nanosheets previously reported by us (cyan trace)[6a] and others (light green trace),[6b] amorphous MoS$_x$ catalysts,[15a] and even shows better performance than a nanocompsite of MoS$_2$ nanoparticles with reduced graphene oxide (RGO).[15b] Furthermore, this overpotential required to achieve j = 10 mA/cm^2 is very competitive among the recently reported non-noble metal catalysts,[1] perhaps only less than that achieved by Ni$_2$P nanoparticles.[1e]
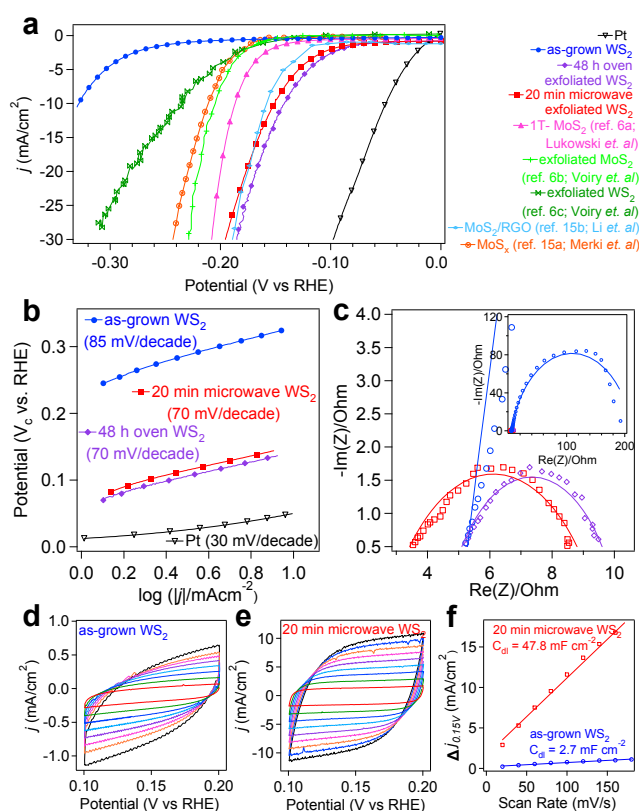
Fig. 3 Electrocatalytic properties of the as-grown and exfoliated WS$_2$. (a) Polarization curves comparing the high-performance HER catalysis from 1T-WS$_2$ nanosheets with the as-grown 2H-WS$_2$ nanostructures, and other reported MX$_2$ catalysts. (b) Corresponding Tafel plots further show the dramatic improvement in catalytic activity after exfoliation. The filled points show the data after iR correction and published data might not have been iR corrected. (c) EIS Nyquist plots collected at a bias voltage of – 0. 250 V vs. RHE show the facile electrode kinetics of the 1T-WS$_2$ nanosheets. Voltammograms of the (d) as-grown and (e) exfoliated WS$_2$ nanosheets at various scan rates (20-180 mV/s) used to (f) estimate the C$_{dl}$ and relative electrochemically active surface area.

Remarkably, the simpler alternative method of microwave-assisted intercalation is equally effective in enhancing the catalytic activity. Exfoliated 1T-WS$_2$ nanosheets produced after only 20 min of microwave-assisted intercalation exhibit nearly equivalent performance, where $j = 10$ mA/cm^2 is reached at –151 mV vs. RHE (red trace with filled squares in Fig. 3a). Measurements carried out on a series of exfoliated WS$_2$ samples that were synthesized in the same batch but subjected to different microwave-assisted intercalation times show the 20 min reaction to be optimal in promoting sufficient lithiation without significant oxidation (Fig. S4). Moreover, the advantages of the harvesting method is apparent after comparing these data with the poor catalytic activity exhibited by samples where growth and exfoliation were carried out on a single graphite substrate where delamination results in significant loss of material (Fig. S5).

The enhanced HER activity is further illustrated by comparing the Tafel slopes (Fig. 3b) of the 1T-WS$_2$ nanosheets (70 mV/decade after *iR* correction for both oven and microwave intercalation) with

the as-grown 2H-WS$_2$ nanostructures (85 mV after *iR* correction). The earlier onset of catalytic activity and lower Tafel slope suggest the free energy of hydrogen binding to 1T-WS$_2$ is closer to equilibrium.[2a] Additionally, we used electrochemical impedance spectroscopy (EIS) to investigate the electrode kinetics under the catalytic HER operating conditions. Nyquist plots (Fig. 3c) and data fittings to a simplified Randles circuit reveal dramatically reduced charge-transfer resistances (R_{ct}) for the exfoliated metallic WS$_2$ nanosheets (6 Ω for the oven intercalation; 5 Ω for the microwave intercalation) in contrast to the as-grown 2H-WS$_2$ nanostructures (200 Ω). Moreover, the small series resistances observed for all samples illustrate that the simple drop-casting method allows high-quality electrical integration of the metallic catalyst with the conductive support.[16] The EIS data confirm that 1T-WS$_2$ nanosheets are highly active catalysts that exhibit facile kinetics toward hydrogen evolution.

We also estimated the relative differences in electrochemically active surface area before and after chemical exfoliation using a simple cyclic voltammetry (CV) method.[17] Current response in the potential window used for the CV (0.1–0.2 V vs. RHE) at different scan rates (20 – 180 mV/s) should be due only to the charging of the double-layer (Fig. 3d, 3e). The double-layer capacitances (C_{dl}) for both samples, which should be directly proportional to the surface area, are extracted by plotting the $\Delta j = j_a - j_c$ at a given potential (0.15 V vs. RHE) against the CV scan rates (Fig. 3f). The proliferation of active sites due to chemical exfoliation is illustrated by the more than an order-of-magnitude increase (a factor of 18) in C_{dl} for the 1T-WS$_2$ nanosheets (48 mF/cm^2) as compared to the as-grown 2H-WS$_2$ nanostructures (2.7 mF/cm^2). While this increase in electrochemically active surface area demonstrates the proliferation of the active sites, which certainly contributes to the improved catalytic performance, the more than two-order-of-magnitude increase in catalytic activity as seen in Fig. 3a and 3b far exceeds the increase of surface area. The dramatic shift in onset potential and the reduction in Tafel slope suggest that the phase transition to the metallic 1T-polymoph is more important to enhancing the catalytic activity. This is consistent with recent results showing exfoliated semiconducting 2H-MoS$_2$ nanosheets exhibited only marginally improved activity,[18] suggesting that the number of edge sites is not the only important factor behind improving the catalytic performance of MX$_2$ materials but the chemical nature of the MX$_2$ nanostructures plays a more importan role in enhancing the HER catalysis, in other words, the metallic 1T nanosheets are instrinsically more catalytically active than the original semiconductor 2H-MX$_2$ nanostructures.

Note that superior HER catalytic performance has been achieved here compared with the metallic WS$_2$ nanosheets chemically exfoliated from commercial WS$_2$ powders.[6c] To better understand this, we carried out side-by-side exfoliation reactions starting from both CVD synthesized WS$_2$ nanostructures and the commercial bulk WS$_2$ powder. Even though both were exposed to identical microwave-assisted intercalation conditions, the nanosheets exfoliated from CVD grown WS$_2$ nanostructures show superior catalytic performance than the nanosheets obtained from the bulk powder (Fig. S6). This is likely first due to incomplete lithium intercalation, conversion, and exfoliation of the bulk WS$_2$ powder, which has larger particle sizes (< 2 μm) and irregular morphologies. Indeed, Raman, PXRD, and SEM data (Fig. S6d-g) show only small

differences in the *n*-butyllithium treated commercial WS_2 powder. Furthermore, even if much longer and harsher intercalation reactions (100 °C for 2 days) were performed on the bulk WS_2 power to result in more complete intercalation as confirmed by SEM and Raman, the catalytic performance of the exfoliated 1T-WS_2 nanosheets originated from bulk power is still inferior to that of the CVD synthesized nanosheets (Fig. S7). This suggests that the few-layer nanostructures with well defined crystalline edges enabled by our CVD synthesis promote better catalytic performance.

Finally, we monitored the catalytic performance of the metastable 1T-WS_2 nanosheets under continuous operation. Even after 500 continuous cycles or nearly 4 h of sustained hydrogen evolution at $j = 10$ mA/cm^2, the catalytic performance of the chemically exfoliated nanosheets remains superior to the as-grown WS_2 nanostructures (Fig. S8). The slow decline in catalytic activity is likely due to the potential loss of the dropcasted material from the surface of the graphite electrode and due to the slow reconversion to the thermodynamically favored 2H-WS_2. To address the latter, the metastable 1T-WS_2 may be further stabilized using various methods, such as tuning the electronic structure via doping.[19]

Conclusions

We have developed methods to significantly enhance the electrocatalytic activity of WS_2 for the HER by controlling its nanostructures and structural polymorphs. Moreover, we demonstrated that microwave-assisted reaction can be used to significantly speed up the intercalation and exfoliation treatment and the exfoliated metallic WS_2 nanosheets can be harvested and drop-casted while still achieving high performance. These facile procedures to chemically exfoliated 1T-WS_2 nanosheets result in favourable kinetics, metallic conductivity, and active site proliferation, which enable the best HER catalytic activity among any MX_2 materials. These results confirm that exfoliation and polymorph control is generally applicable for enhancing the catalytic and other applications of the family of MX_2 materials.

Acknowledgements

Notes and references

a Department of Chemistry, University of Wisconsin-Madison, 1101 University Ave., Madison, Wisconsin 53706, USA. * Email: jin@chem.wisc.edu.

† Electronic Supplementary Information (ESI) available: experimental details, additional structural characterization, HER catalytic performance comparison with exfoliated nanosheets from bulk commercial WS_2 powers, and stability of catalytic activity. See DOI: 10.1039/c000000x/

1 (a) J. A. Turner, *Science*, 2004, **305**, 972-974; (b) N. S. Lewis and D. G. Nocera, *Proc. Natl. Acad. Sci. U. S. A.*, 2006, **103**, 15729-15735; (c) J. R. McKone, E. L. Warren, M. J. Bierman, S. W. Boettcher, B. S. Brunschwig, N. S. Lewis and H. B. Gray, *Energ Environ Sci*, 2011, **4**, 3573-3583; (d) W.-F. Chen, K. Sasaki, C. Ma, A. I. Frenkel, N. Marinkovic, J. T. Muckerman, Y. Zhu and R. R. Adzic, *Angew. Chem. Int. Ed.*, 2012, **51**, 6131-6135; (e) E. J. Popczun, J. R. McKone, C. G. Read, A. J. Biacchi, A. M. Wiltrout, N. S. Lewis and R. E. Schaak, *J. Am. Chem. Soc.*, 2013, **135**, 9267-9270; (f) W. F. Chen, C. H. Wang, K. Sasaki, N. Marinkovic, W. Xu, J. T. Muckerman, Y. Zhu and R. R. Adzic, *Energy Environ. Sci.*, 2013, **6**, 943-951; (g) B. Cao, G. M. Veith, J. C. Neuefeind, R. R. Adzic and P. G. Khalifah, *J. Am. Chem. Soc.*, 2013, **135**, 19186-19192.

2 (a) A. B. Laursen, S. Kegnaes, S. Dahl and I. Chorkendorff, *Energy Env. Sci.*, 2012, **5**, 5577-5591; (b) D. Merki and X. Hu, *Energ Environ Sci*, 2011, **4**, 3878-3888; (c) J. Yang and H. S. Shin, *J. Mater. Chem. A*, 2014, 2, 5979-5985.

3 T. F. Jaramillo, K. P. Jørgensen, J. Bonde, J. H. Nielsen, S. Horch and I. Chorkendorff, *Science*, 2007, **317**, 100-102.

4 B. Hinnemann, P. G. Moses, J. Bonde, K. P. Jørgensen, J. H. Nielsen, S. Horch, I. Chorkendorff and J. K. Nørskov, *J. Am. Chem. Soc.*, 2005, **127**, 5308-5309.

5 (a) Z. Wu, B. Fang, A. Bonakdarpour, A. Sun, D. P. Wilkinson and D. Wang, *Applied Catalysis B: Environmental*, 2012, **125**, 59-66; (b) A. Sobczynski, A. Yildiz, A. J. Bard, A. Campion, M. A. Fox, T. Mallouk, S. E. Webber and J. M. White, *J. Phys. Chem.*, 1988, **92**, 2311-2315; (c) J. Bonde, P. G. Moses, T. F. Jaramillo, J. K. Norskov and I. Chorkendorff, *Faraday Discussions*, 2009, **140**, 219-231; (d) J. Kim, S. Byun, A. J. Smith, J. Yu and J. Huang, *J. Phys. Chem. Lett.*, 2013, **4**, 1227-1232; (e) J. Yang, D. Voiry, S. J. Ahn, D. Kang, A. Y. Kim, M. Chhowalla and H. S. Shin, *Angew. Chem. Int. Ed.*, 2013, **52**, 13751-13754.

6 (a) M. A. Lukowski, A. S. Daniel, F. Meng, A. Forticaux, L. Li and S. Jin, *J. Am. Chem. Soc.*, 2013, **135**, 10274-10277; (b) D. Voiry, M. Salehi, R. Silva, T. Fujita, M. Chen, T. Asefa, V. B. Shenoy, G. Eda and M. Chhowalla, *Nano Lett.*, 2013, **13**, 6222-6227; (c) D. Voiry, H. Yamaguchi, J. Li, R. Silva, D. C. B. Alves, T. Fujita, M. Chen, T. Asefa, V. B. Shenoy, G. Eda and M. Chhowalla, *Nat. Mater.*, 2013, **12**, 850-855; (d) H. Wang, Z. Lu, S. Xu, D. Kong, J. J. Cha, G. Zheng, P.-C. Hsu, K. Yan, D. Bradshaw, F. B. Prinz and Y. Cui, *Proc. Natl. Acad. Sci. U. S. A.*, 2013, **110**, 19701-19706.

7 (a) X. Huang, Z. Zeng and H. Zhang, *Chem. Soc. Rev.*, 2013, **42**, 1934-1946; (b) X. Huang, Z. Zeng, S. Bao, M. Wang, X. Qi, Z. Fan and H. Zhang, *Nature Commun.*, 2013, **4**, 1444.

8 (a) P. Joensen, R. F. Frindt and S. R. Morrison, *Mater. Res. Bull.*, 1986, **21**, 457-461; (b) D. Yang and R. F. Frindt, *J. Phys. Chem. Solids*, 1996, **57**, 1113-1116; (c) G. Eda, H. Yamaguchi, D. Voiry, T. Fujita, M. Chen and M. Chhowalla, *Nano Lett.*, 2011, **11**, 5111-5116.

9 (a) Z. Zeng, Z. Yin, X. Huang, H. Li, Q. He, G. Lu, F. Boey and H. Zhang, *Angew. Chem. Int. Ed.*, 2011, **50**, 11093-11097; (b) Z. Zeng, C. Tan, X. Huang, S. Bao and H. Zhang, *Energy Env. Sci.*, 2014, **7**, 797-803.

10 B. K. Miremadi and S. R. Morrison, *J. Appl. Phys.*, 1988, **63**, 4970-4974.

11 E. Benavente and G. González, *Mater. Res. Bull.*, 1997, **32**, 709-717.

12 (a) K. E. Dungey, M. D. Curtis and J. E. Penner-Hahn, *Chem. Mater.*, 1998, **10**, 2152-2161; (b) H.-L. Tsai, J. Heising, J. L. Schindler, C. R. Kannewurf and M. G. Kanatzidis, *Chem. Mater.*, 1997, **9**, 879-882; (c) J. Heising and M. G. Kanatzidis, *J. Am. Chem. Soc.*, 1999, **121**, 638-643.

Energy & Environmental Science Accepted Manuscript

13 R. Bhandavat, L. David and G. Singh, *J. Phys. Chem. Lett.*, 2012, **3**, 1523-1530.

14 H. S. S. Ramakrishna Matte, A. Gomathi, A. K. Manna, D. J. Late, R. Datta, S. K. Pati and C. N. R. Rao, *Angew. Chem.*, 2010, **122**, 4153-4156.

15 (a) D. Merki, S. Fierro, H. Vrubel and X. Hu, *Chemical Science*, 2011, **2**, 1262-1267; (b) Y. Li, H. Wang, L. Xie, Y. Liang, G. Hong and H. Dai, *J. Am. Chem. Soc.*, 2011, **133**, 7296-7299.

16 M. S. Faber, K. Park, M. Cabán-Acevedo, P. K. Santra and S. Jin, *J. Phys. Chem. Lett.*, 2013, **4**, 1843-1849.

17 D. Merki, H. Vrubel, L. Rovelli, S. Fierro and X. Hu, *Chem Sci*, 2012, **3**, 2515-2525.

18 P. Ge, M. D. Scanlon, P. Peljo, X. Bian, H. Vubrel, A. O'Neill, J. N. Coleman, M. Cantoni, X. Hu, K. Kontturi, B. Liu and H. H. Girault, *Chem. Commun.*, 2012, **48**, 6484-6486.

19 A. N. Enyashin, L. Yadgarov, L. Houben, I. Popov, M. Weidenbach, R. Tenne, M. Bar-Sadan and G. Seifert, *J. Phys. Chem. C*, 2011, **115**, 24586-24591.

Table of Content Entry

Metallic WS$_2$ nanosheets chemically exfoliated from chemical vapour deposited WS$_2$ nanostructures display excellent catalytic activity for the hydrogen evolution reaction.